Journal of Biomedical Optics

BiomedicalOptics.SPIEDigitalLibrary.org

Particle swarm optimization method for small retinal vessels detection on multiresolution fundus images

Bilal Khomri
Argyrios Christodoulidis
Leila Djerou
Mohamed Chaouki Babahenini
Farida Cheriet

SPIE.

Bilal Khomri, Argyrios Christodoulidis, Leila Djerou, Mohamed Chaouki Babahenini, Farida Cheriet, "Particle swarm optimization method for small retinal vessels detection on multiresolution fundus images," *J. Biomed. Opt.* **23**(5), 056004 (2018), doi: 10.1117/1.JBO.23.5.056004.

Particle swarm optimization method for small retinal vessels detection on multiresolution fundus images

Bilal Khomri,[a,b,*] Argyrios Christodoulidis,[b] Leila Djerou,[a] Mohamed Chaouki Babahenini,[a] and Farida Cheriet[b]
[a]University of Biskra, LESIA Laboratory, Biskra, Algeria
[b]Polytechnique Montréal, LIV4D Laboratory, Montréal, Québec, Canada

Abstract. Retinal vessel segmentation plays an important role in the diagnosis of eye diseases and is considered as one of the most challenging tasks in computer-aided diagnosis (CAD) systems. The main goal of this study was to propose a method for blood-vessel segmentation that could deal with the problem of detecting vessels of varying diameters in high- and low-resolution fundus images. We proposed to use the particle swarm optimization (PSO) algorithm to improve the multiscale line detection (MSLD) method. The PSO algorithm was applied to find the best arrangement of scales in the MSLD method and to handle the problem of multiscale response recombination. The performance of the proposed method was evaluated on two low-resolution (DRIVE and STARE) and one high-resolution fundus (HRF) image datasets. The data include healthy (H) and diabetic retinopathy (DR) cases. The proposed approach improved the sensitivity rate against the MSLD by 4.7% for the DRIVE dataset and by 1.8% for the STARE dataset. For the high-resolution dataset, the proposed approach achieved 87.09% sensitivity rate, whereas the MSLD method achieves 82.58% sensitivity rate at the same specificity level. When only the smallest vessels were considered, the proposed approach improved the sensitivity rate by 11.02% and by 4.42% for the healthy and the diabetic cases, respectively. Integrating the proposed method in a comprehensive CAD system for DR screening would allow the reduction of false positives due to missed small vessels, misclassified as red lesions. [DOI: 10.1117/1.JBO.23.5.056004]

Keywords: retinal blood vessel segmentation; fundus imaging; multiscale line detection; multiobjective optimization; particle swarm optimization algorithm; image segmentation.

Paper 170826R received Dec. 22, 2017; accepted for publication Apr. 10, 2018; published online May 10, 2018.

1 Introduction

The extraction of the retinal vasculature from fundus images is an important step for the diagnosis of eye diseases. The inspection of the retinal vessels is considered an integral part of the medical examination in ophthalmology. Possible morphological changes in the appearance of the vascular structures in the retinal image can be the result of manifestations of many systemic diseases, such as cardiovascular[1] or diabetes[2] pathologies. As an example, the vessel caliber can act as a biomarker for coronary heart diseases,[3] and the growth of new vessels is considered as a landmark for the transition of a retinopathy to the proliferative stage, which is related to high risk of blindness. According to the World Health Organization,[4] diabetic retinopathy (DR) is the leading cause of blindness in developed countries, and it is estimated that 4.8% of 37 million diabetic patients become blind due to DR. Worldwide, 333 million diabetic patients in the next 10 years will require retinal examination each year, which will greatly increase the workload on ophthalmologists. To cover larger populations and reduce the disease's impact through earlier detection, computer-aided diagnosis (CAD) systems have been proposed to assign the patients to different eye-care specialists depending on the type of treatment required and to reduce the patient/ophthalmologist ratio. The automatic segmentation of retinal vessels is usually the first step in a CAD system.[5] In addition, this information is provided to the physician to assist him in clinical assessment of many other pathologies. For example, vessel segmentation is a prerequisite step in the evaluation of retinopathy of prematurity,[6] extraction of measurements on the vessel diameters,[7] detection of the fovea region,[8] detection of arteriolar narrowing,[9] or even in computer-assisted laser therapy of retinopathies.[10] Thus, even if many algorithms were proposed in the literature for an automatic detection of retinal lesions in fundus images without retinal vessel segmentation,[11–15] an accurate segmentation of small retinal vessels is still needed for assessment of other diseases.

A considerable amount of work on the automatic retinal vessel segmentation problem has been reported in the literature.[16] The available methods can be classified into two main categories: supervised[17–22] or unsupervised.[23–34] Supervised methods utilize classifiers to categorize image pixels as belonging to either retinal vessels or background (nonvessel). Various types of classifiers based on machine-learning methods have been proposed in the literature to classify the different regions of interest from a set of extracted features. Among these, support vector machines,[17] artificial neural networks,[18] the K-nearest neighbors,[19] lattice neural networks,[20] and the Gaussian mixture models[21] have been used. Lately, deep-learning classifiers have been proposed, such as convolutional neural networks,[22] in order to avoid the extraction of handcrafted features. Overall, the recent methods based on supervised learning provide good results. However, the performance of the algorithms

*Address all correspondence to: Bilal Khomri, E-mail: bilal.khomri@polymtl.ca

1083-3668/2018/$25.00 © 2018 SPIE

depends on the careful tuning of its parameters, which increases its training time. Second, the methods require a manually labeled set by an expert, which is a very tedious and time-consuming task.[19] On the other hand, the unsupervised approaches attempt to find the blood vessels in the retinal images without any prior labeling information. The different proposed methods are categorized into either clustering or intensity-based techniques. Clustering[32,33] is the most widely investigated approach, in which a feature-designed space is used and the pixels are classified into two clusters, either vessel or nonvessel, based on their relative distance in the feature space. The features are extracted from intensity-based characteristics, such as the grayscale level, the gradient, the local texture, or the derivatives. Intensity-based methods consist of detecting the vessels by identifying specific image patterns that discriminate the vessels from other structures. These include the morphological operators,[23] model-based methods,[24] matched filtering (MF),[25] multiscale line detector methods,[26] vessel tracking,[27] multiscale vessel segmentation methods,[28] and bioinspired algorithms/heuristics-metaheuristics.[29–34] However, the existing clustering methods require the correct initialization of a predefined number of clusters to avoid the trapping of the cluster centeres into a local minimum. For the intensity-based methods, the drawback is that sophisticated approaches have to be employed to deal with a crossover or bifurcation point due to the complexity of the intensity profile at these regions. Since vessel crossover or branching points are not well displayed, these methods usually tend to terminate at these points, and this leads to the incompleteness in the detection of all vessels.[26]

Thus, blood-vessel segmentation from retinal images is still a challenging task, even if several line detection methods have been proposed to resolve this problem.[35] Based on the basic line detector, Nguyen et al.[26] proposed the multiscale line detection method (MSLD) in order to accommodate the various vessel sizes that appear in the retinal image. This method is considered as the most effective approach in the segmentation of the large- and medium-sized vessels compared to existing methods. However, the MSLD method does not take into account the fact that blood vessels generally yield the optimal line response in a specific scale that corresponds to their specific size. The method uses all the available scales exhaustively, which is expensive. Moreover, small vessels' line response decreases when higher scales are used, because a large averaging area is performed to normaliz the overall response. Recently, Christodoulidis et al.[36] proposed a hybrid approach based on the combination of the tensor-voting framework[37] and the MSLD method, in order to overcome the limitations of this approach in handling the smallest vessels. However, the time complexity of this approach is very high compared to other methods.

On the other hand, several nature-inspired optimization algorithms have been proposed for the segmentation of retinal blood vessels. However, most of the existing bioinspired algorithms do not take into account the different characteristics of the thin and the large vessels in their optimization process, because they use only a single criterion based on a specific feature. For example, a genetic algorithm is used by Al-Rawi and Karajeh[29] to obtain the optimum thresholding parameters for the MF response. Cinsdikici and Aydın[30] used an ant colony algorithm and a hybrid model of the MF to reduce the strong response from the boundary of the bright or dark diabetic lesions, which in turn reduce the false positives (FPs). Moreover, Asad et al.[31] proposed a new feature selection approach based on ant colony optimization in order to minimize the classification complexity by removing redundant features. In Ref. 32, the probabilistic fuzzy c-means (FCM) clustering objective function is optimized by a cuckoo search technique to find the best segmentation.

Even though many promising methods based on nature-inspired optimization algorithms have been proposed in the literature, the methods can be improved by taking into account local context information. Recently, Hassanien et al.[33] and Emary et al.[34] showed that the inclusion of several criteria in the segmentation phase gives satisfactory results and helps to extract the thin vessels. In Ref. 33, for example, the proposed algorithm is based on two levels of clustering. At the first level, the artificial bee colony (ABC) optimization algorithm on the FCM function was used to localize medium-diameter vessels. At the second level, the obtained cluster centeres were enhanced using a pattern search optimization approach with emphasis on localizing small-diameter vessels, where the thinnest ratio was used as a fitness function for the pattern search algorithm. In Ref. 34, an algorithm was proposed based on the flower-pollination-search (FPSA) and the pattern-search (PS) algorithms. As a first step, the FPSA algorithm searches the full vasculature from the retinal images, then the PS algorithm is used to localize the thin vessels that are not identified by the first optimization algorithm. However, the limitation of these methods is that they optimize the different criteria separately by using different optimization algorithms, which is time-consuming. Nevertheless, particle swarm optimization (PSO) techniques have been able to outperform standard algorithms for segmentation of biomedical images.[38]

In our previous preliminary work,[39] we applied the PSO algorithm to improve the MSLD method for the retinal blood-vessel segmentation problem. The PSO algorithm was adapted to find the best scales in the MSLD method. The proposed method demonstrated fast convergence to the optimal solution, with better vessel segmentation than the MSLD method, using fewer scales. However, the initialization step, which consists in choosing two specific scales representing the size of small and large vessels, negatively affects the optimization convergence of the algorithm, due to the limitation of the search space of the PSO algorithm. In addition, the method did not take into account the line response recombination problem of the various scales in the MSLD method. Finally, the segmentation performance was validated only on healthy subjects from a single public high-resolution fundus (HRF) image database.

In this work, we exploited the flexibility of multiobjective fitness functions and the power of the PSO algorithm to find the best arrangement of the available scales and to overcome the drawbacks of the scale response recombination in the MSLD method. The sensitivity and the specificity measures were used simultaneously as objective functions, in order to evaluate the result of the PSO algorithm at each iteration. To validate experimentally the performance of the proposed method, two low-resolution fundus and one HRF image datasets were used.

The organization of this paper is as follows. Section 2 presents the concepts of the proposed retinal blood vessel segmentation algorithm. In Sec. 3, we discuss the experimental results obtained from applying the proposed method on three widely used publicly available retinal image datasets. Finally, the conclusion is given in Sec. 4.

2 Method

The method used to extract the vessels from the retinal images is described in this section. First, we introduce the algorithm proposed by Nguyen et al.,[26] which represents the first step of our method. Then, we present the basic concepts of the PSO algorithm. The proposed method involves the process of finding the best arrangement of the line-detection scales, by application of the PSO algorithm (Sec. 2.3). Finally, the proposed recombination step is presented in Sec. 2.4.

2.1 *Multiscale Line Detection Algorithm*

The MSLD method[26] is a generalized model of the single-scale line detection method.[17] As first proposed, it uses a straight sampling segment of variable length L that is rotated around a central pixel. The mean intensity along the segment is computed with the goal of maximizing its response $I^L_{\max}$ when the segment is parallel to the vessel direction. The maximum response is then corrected by comparing it against the average intensity I^w_{avg} in the neighborhood of the central pixel. The size of the neighborhood W equals the highest chosen scale or line length. The line response for a single scale is computed as follows:

$$R^L_{\max} = I^L_{\max} - I^w_{\text{avg}}. \tag{1}$$

According to the authors,[26] the chosen length of the scale parameter W is twice the diameter of a typical vessel in the retinal image. Thus, a high-resolution image, as in the HRF) database,[40] requires a value close to $W = 40$ pixels with a scale-increasing step of two. In contrast, for a low-resolution image, as in the DRIVE database,[19] half the previous value is sufficient. To get the final MSLD response, the following equation [Eq. (2)] is used to calculate the linear combination of the line responses across all the available scales

$$R_{\text{combined}} = \frac{1}{n_L + 1}\left(\sum_L R^L_W + I_{\text{igc}}\right), \tag{2}$$

where n_L is the number of scales, R^L_W is the response of the line detector at scale L, and I_{igc} is the value pixel of the inverted green channel.

2.2 *Particle Swarm Optimization Algorithm*

The PSO algorithm is an evolutionary computation technique proposed by Eberhart and Kennedy.[41] The advantage of PSO is that it is simple in concept, easy to implement, and there are very few control parameters to adjust in comparison with other evolutionary techniques. The method is used for stochastic optimization and is similar to the swarm intelligence principles observed in natural behaviors of groups of animal species. These are known collectively as swarms, and they can include flocks of birds, or even the sociological behavior of a group of people.[42] Each individual of the swarm is represented by a particle. In the PSO algorithm, the particle candidates are called solutions. To find an optimal solution, the particles travel through the search space and follow the particles that are at their previous best positions, as well as near food sources. In each step of the PSO procedure, $\overline{\text{gbest}}_i$ is the global best value obtained thus far by any particle in the population when the entire swarm is updated. For each iteration of the algorithm, the new position of a particle is computed according to its previous position $\overline{X}_i$, velocity $\overline{V}_i$, or rate of position change, and $\overline{\text{gbest}}_i$ value. This is an iterative process that is repeated until a predefined convergence criterion is met. Algorithm 1 presents the basic stages of the PSO algorithm.

Algorithm 1. The basic stages of the PSO algorithm

Initialize swarm (Initialize $\overline{X}_i$, $\overline{V}_i$ and $\overline{\text{gbest}}_i$)

Loop:

  For all particles

    Evaluate the Fitness function ($\bar{f}_i$) of each particle $\overline{X}_i$

    Update $\overline{X}_i$, $\overline{V}_i$, and $\overline{\text{gbest}}_i$

    Update the new position $\overline{X}_i$

  End

Until stopping criteria (convergence)

2.3 *Proposed Scale Rearrangement Algorithm*

Our main contribution is the optimization of the arrangement of the available scales in the MSLD method by exploiting the flexibility of the PSO algorithm. In the MSLD method, all the available scales between the minimum and the maximum are usually considered for any vessel size. This is deficient because vessels generally yield the optimal line response at a particular scale that depends on their diameter. In the proposed algorithm, we select the most optimal scales and retain only those that contribute to the overall optimization of the objective functions.

In our application, we assume that the retinal images contain three calibers of vessels: (1) small, (2) large, and (3) medium range of vessels (Fig. 1). According to the diagram (Fig. 2), at the initialization step we assign each particle ($\overline{X}_i$) to a specific scale among the three available vessel calibers. The optimization process is iterative. At the second step, we add a new scale for each particle in order to extract more vessels from the retinal image. Then, we compare the new particle with the previous particle according to its position $\overline{X}_i$ using the objective functions. In our case, the objective functions that we use represent the sensitivity and the specificity of the segmented image [Eqs. (4) and (5)]. We sort the particles, in order to keep only the best for each iteration, by applying the multiobjective optimization strategies proposed by Huo et al.,[43] namely the fast, nondominated sorting method, and the population selection strategy. At the end of the process, we keep the best particle that gave the best scales.

2.4 *Proposed Recombination Algorithm*

Additionally, we propose to cluster the identified scales depending on their contribution to the detection of each vessel. We aim to avoid the negative impact of combining scales at lower or at higher level than the optimal for a vessel of a specific size. The proposed process of scale recombination is demonstrated in Fig. 3.

In the MSLD approach, the final recombination response depends on the number of the available scales [Eq. (2)], with the method equally weighting the contribution of each scale.

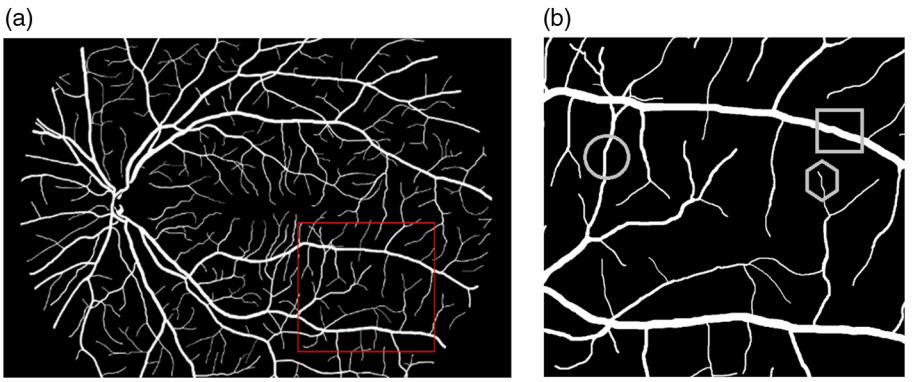

Fig. 1 Example of the three different considered calibers of vessels in the retinal vessels. (a) Reference segmentation from a high-resolution retinal image (HRF);[40] (b) zoomed region corresponding to the red square inset in (a); rectangle form indicates the large vessels, hexagon form shows the small vessels, while oval form indicates the medium caliber vessels.

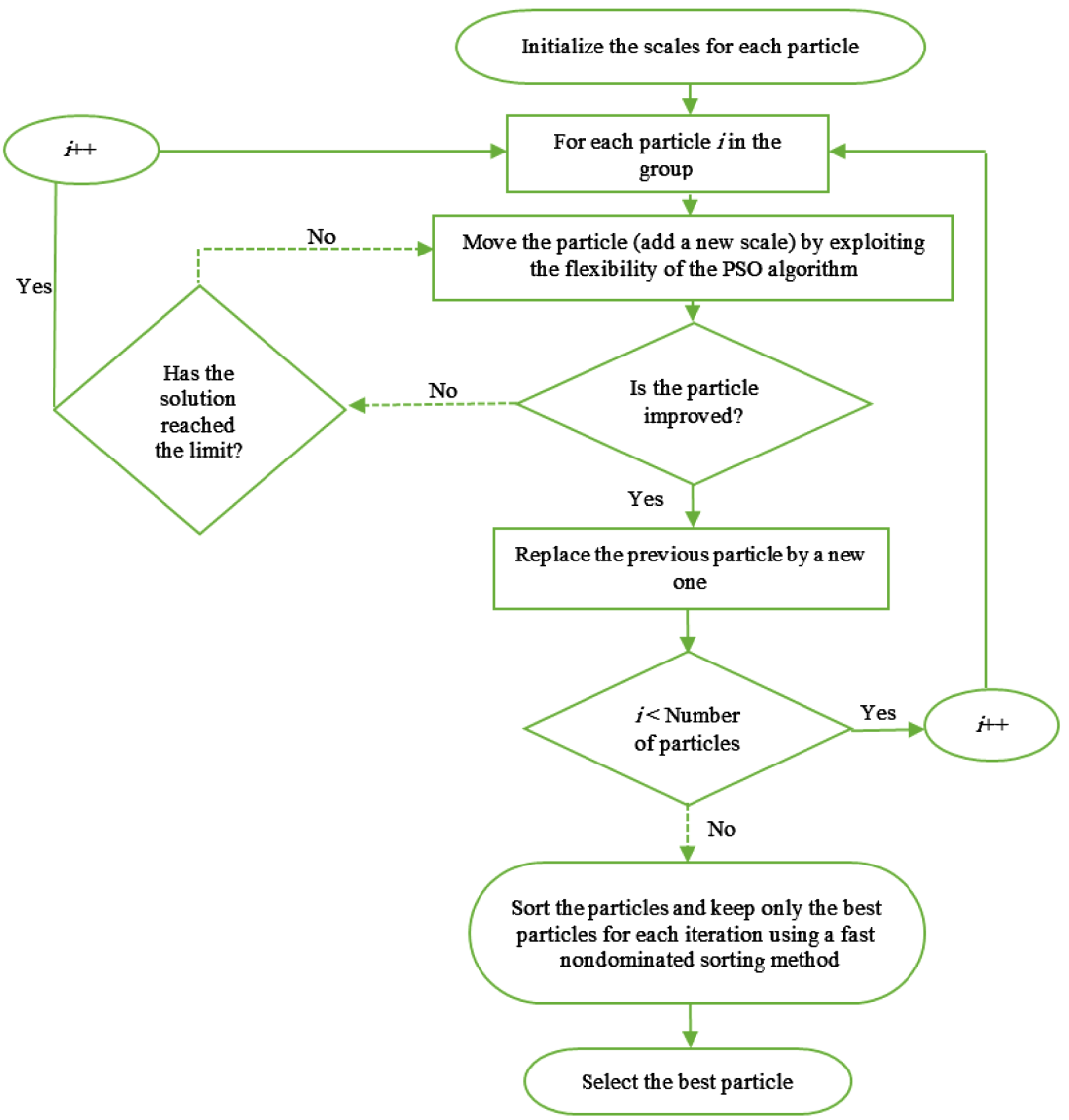

Fig. 2 Flowchart of the process for selecting the best scales by the PSO algorithm.

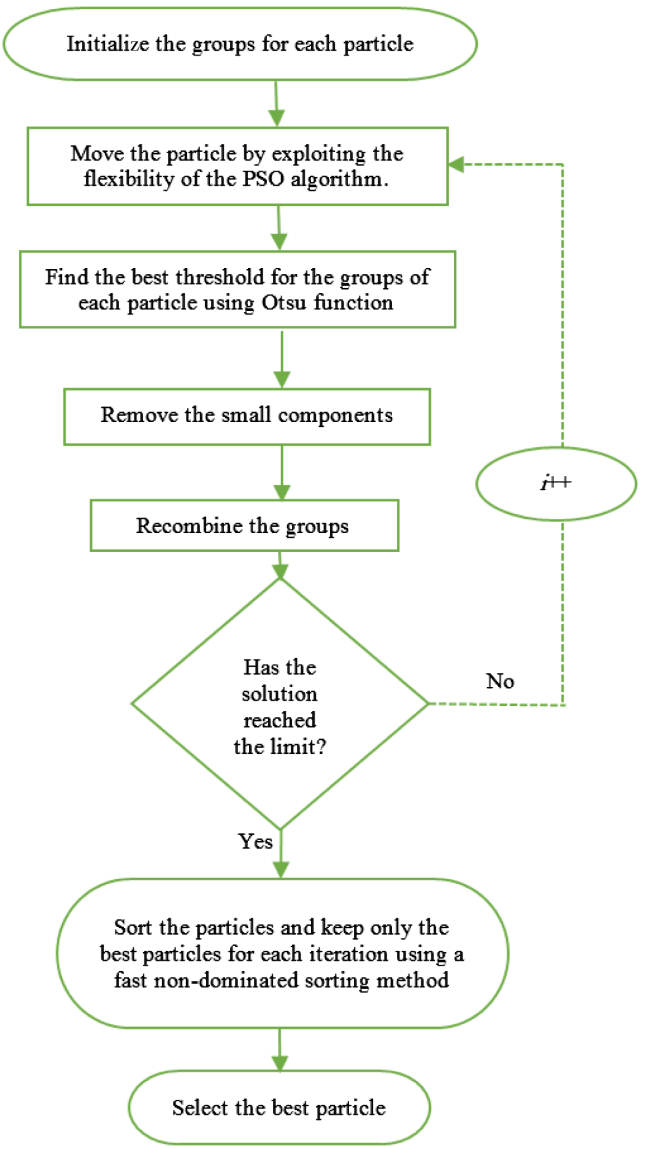

Fig. 3 Flowchart of the proposed recombination method.

However, this is not optimal because contributions from some scales that are not relevant for the examined vessels, and the correction against the averaging neighborhood [Eq. (1)] can reduce the overall line-detection response. For example, in the recombination phase, small vessels' line response decreases when high scales in the cluster are used, because the line response is corrected based on the use of a large averaging. In certain regions, at the periphery and the center of the retina, the contrast between the small vessels and the background is low. Moreover, the small vessels are thin and appear tortuous, and their morphology could be affected in pathological cases. When the MSLD approach is applied to this category of vessels, there is an overall reduction in the recombined multiscale line response R_{Combined}, which is a combination of two factors. First, the length of the sampling line at high scales exceeds the size of the small vessels, and so the overall mean $I^{L}_{\max}$ is normalized by background pixels adjacent to the vessels.

Second, the averaging window from large scales considers a significant number of background pixels, which overall increases the value of I^{w}_{avg}. Therefore, the final MSLD response value is reduced at low-contrast regions with small vessels. Equally, large vessels central line response decreases when lower scales in the cluster are used because of the small averaging area that fits completely inside the vessel. The PSO algorithm is a suitable alternative to cluster the scales depending on the size of vessels. To do so, we searched the best threshold for each cluster Gr_i, and removed the small components from the segmented results. Finally, we recombined the results according to the following equation:

$$Gr_{\text{Combined}} = \frac{1}{n}(Gr_i + Gr_{i+1} + \cdots + Gr_n), \tag{3}$$

where n is the number of clusters.

For the classification of a region as vessel or background, we used Otsu's method to find the best threshold that increases the separation between the two classes, so that their combined spread is minimal.[44] Since small isolated background linear structures can be misclassified as blood vessel, we applied morphological area opening (see Fig. 4) to suppress all connected components that had fewer than P pixels area size. The choice of the value of the parameter P is empirical and should be adapted to the given database.

3 Experimental Results and Discussion

3.1 *Datasets and Performance Measures*

Three databases are considered to evaluate the performance of the proposed method: DRIVE[19] and STARE[25] databases for the low-resolution images and HRF[40] database for the HRF images.

DRIVE dataset contains 40 images with an image size of 584×565 pixels obtained at 45 deg field of view (FOV). This dataset is further separated into a DRIVE training set and a DRIVE test set with 20 images in each set. The DRIVE test set is annotated by two experts, whereas the training set is annotated by a single expert. The images were obtained from a DR screening program in the Netherlands. The screening population consisted of 453 subjects between 31- and 86-years old. The STARE dataset contains 20 images with an image size of 605×700 obtained at 35 deg FOV, which are manually annotated by two independent human experts. In this case, 10 images represent patients with retinal abnormalities (STARE abnormal). The other 10 images represent healthy retinas (STARE normal). These datasets containing manual segmentations by experts are considered as the gold standard.

Recently, high-resolution images are becoming more common in clinical practice; thus, in our work we also evaluated the performance of the proposed method on high-resolution images. The Erlangen HRF database has been newly established by a collaborative research group; the database contains 15 images of healthy (H), 15 images of DR, and 15 images of glaucomatous (G) eyes. The images were acquired using a CANON CF-60UVi camera with fixed image resolution of 3504×2336 pixels. Manual segmentations of the vessels by an expert are also available for the three categories of images.

Based on these gold standards from the low- and high-resolution databases, we calculated the sensitivity (Sen), specificity (Spec), and accuracy (Acc) of the proposed method. The sensitivity [Eq. (4)] quantifies the ability of the algorithm to detect correctly the vessel pixels, whereas the specificity [Eq. (5)] quantifies the ability of the algorithm to identify correctly non-vessel pixels, or the background. Finally, accuracy [Eq. (6)] is

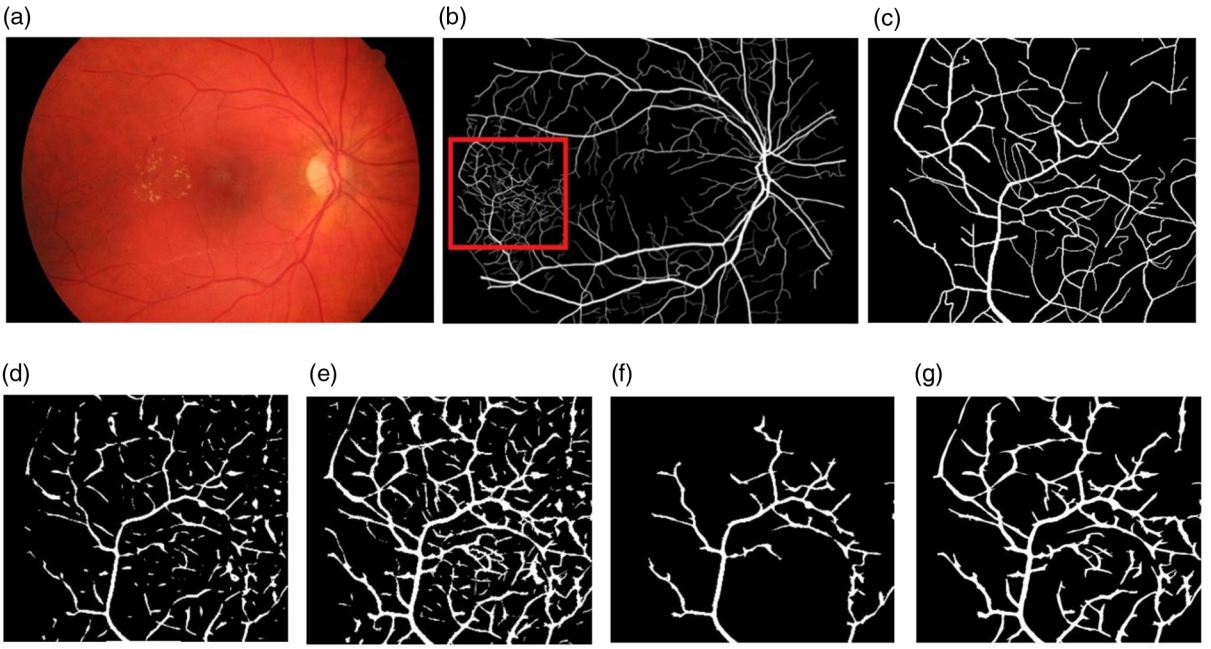

Fig. 4 Effect of the threshold and the postprocessing steps on the final segmentation result in (image 06 DR case, HRF datasets): (a) the diabetic fundus image; (b) ground-truth segmentation image; (c) ground-truth segmentation corresponding to the red square inset in (b); (d) and (e) the segmentation by the MSLD and the proposed algorithms, respectively; and (f) and (g) the effect of the postprocessing on the final segmentation for the MSLD approach and the proposed method, respectively.

the ratio of the total number of correctly classified pixels to the number of pixels in the image FOV

$$\text{Sensitivity} = \frac{\text{TP}}{\text{TP} + \text{FN}}, \tag{4}$$

$$\text{Specificity} = \frac{\text{TN}}{\text{TN} + \text{FP}}, \tag{5}$$

$$\text{Accuracy} = \frac{\text{TP} + \text{TN}}{\text{TP} + \text{FN} + \text{FP} + \text{TN}}, \tag{6}$$

where TP, TN, FP, and FN are true positive, true negative, false positive, and false negative, respectively.

3.2 *Performance Evaluation*

To compare the results of the proposed method with those of the MSLD method,[26] and other state-of-the-art methods, the performance of the vessels' segmentation was evaluated separately on the low- and high-resolution databases. To tune the parameters of the proposed method, DRIVE training set and HRF glaucomatous set were used, respectively. In the MSLD method, the maximum line length W is fixed to 40 pixels for the high-resolution images, and 15 pixels for the low-resolution images. This choice is based on the rule-of-thumb of using a length twice the width of an average vessel in an image. In the proposed method, the value of W is fixed for each cluster of scales based on the flexibility of the PSO algorithm, and the setting of the maximum line length parameter is adaptive. The PSO algorithm was optimized for 50 iterations and population size 100. For the evaluation of the execution time, we used a personal computer with a 2.6-GHz processor and 4 GB RAM.

3.2.1 *Performance evaluation on the high-resolution dataset*

The existing work on vessel segmentation has been validated on low-resolution datasets only.[29–34] Instead, in this study, we also considered a high-resolution dataset in order to demonstrate the effectiveness of the proposed method on different retinal image resolutions. In our experiment, the healthy (H) and the DR groups were used to compare the MSLD and the proposed methods. After the application of the proposed method, the algorithm partitions the available scales into three clusters (L_1, L_2, L_3) with: $L_1 = \{3, 7, 9\}$, $L_2 = \{13, 15, 19, 21\}$, and $L_3 = \{25, 27, 37\}$. Subsequently, the thresholds for each cluster are set to $T_{L1} = 0.65$, $T_{L2} = 0.75$, and $T_{L3} = 0.48$, while the threshold value used for the MSLD method is $T = 0.63$.

Overall, the number of scales was reduced from 21 to 10. Qualitatively, from the binarized images in Figs. 4(d) and 4(e), we can see the effectiveness of using a specific threshold for each cluster of scales compared to the case where a common threshold across all the scales is used. The proposed method extracts the vessels more reliably than does the MSLD method and with less background noise. We can conclude that the choice of a single threshold for all scales is not sufficient to segment well the different sizes of retinal vessels. Furthermore, the choice of the threshold value is performed manually in the MSLD method, whereas the proposed method selects the thresholds automatically based on the optimization of the final segmentation. The robustness of the proposed method was evaluated quantitatively according to two strategies: first, when the full vasculature is considered and second, when separating the large and the small vessels.

Full vasculature analysis and comparison. Table 1 shows the results in terms of standard discrepancy metrics

Table 1 Full vasculature performance comparison on the test set in terms of sensitivity, specificity, and accuracy.

Method	Sensitivity ($\mu \pm \sigma$)	Specificity ($\mu \pm \sigma$)	Accuracy ($\mu \pm \sigma$)	Time (min)
MSLD method	82.58% ± 3.65%	95.40% ± 2.14%	94.13% ± 1.72%	3.31
Proposed method	87.09% ± 3.46%	95.40% ± 1.78%	94.54% ± 1.51%	3.27

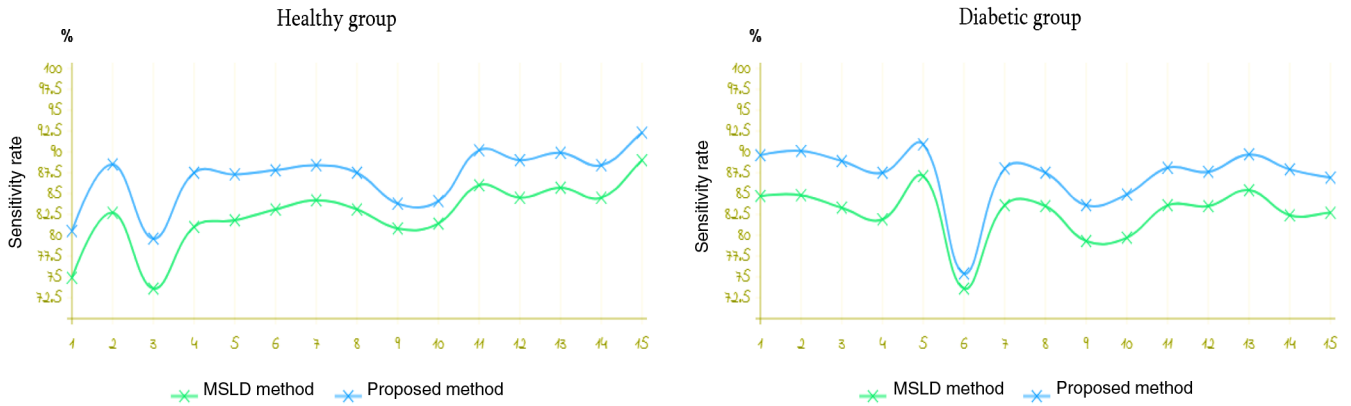

Fig. 5 Per image performance comparison of the sensitivity rate on the healthy and diabetic groups.

in the healthy and the diabetic group of images. The proposed methods achieved segmentation of more vessels than the MSLD. The proposed method improved the sensitivity rate for the full vasculature segmentation against the MSLD by 4.51% for the test set. Figure 5 demonstrates the per image performance sensitivity rate of the proposed and the MSLD methods on the H and DR datasets. From these two graphs, we can see that the proposed method achieved a consistently higher sensitivity rate than the MSLD method. The difference is stable regardless whether the image is healthy or contains various types of lesions such as MAs, exudates, hemorrhages, or neovascularization.

Figure 6 shows qualitative results on the segmentation of healthy and diabetic images for the two compared methods. The two examples demonstrate the robustness of the proposed method compared to the MSLD approach. In the case of the diabetic image, we can see that some abnormalities, consisting mainly of lesions and linear background structures, are isolated when the MSLD method is applied. However, the proposed method handled this problem by reducing the response from background structures. For vessels with small diameters, the MSLD method provides low line-response values, mainly because the scales are not correctly rearranged, or recombined. Similarly, for the healthy case, we can see that the proposed

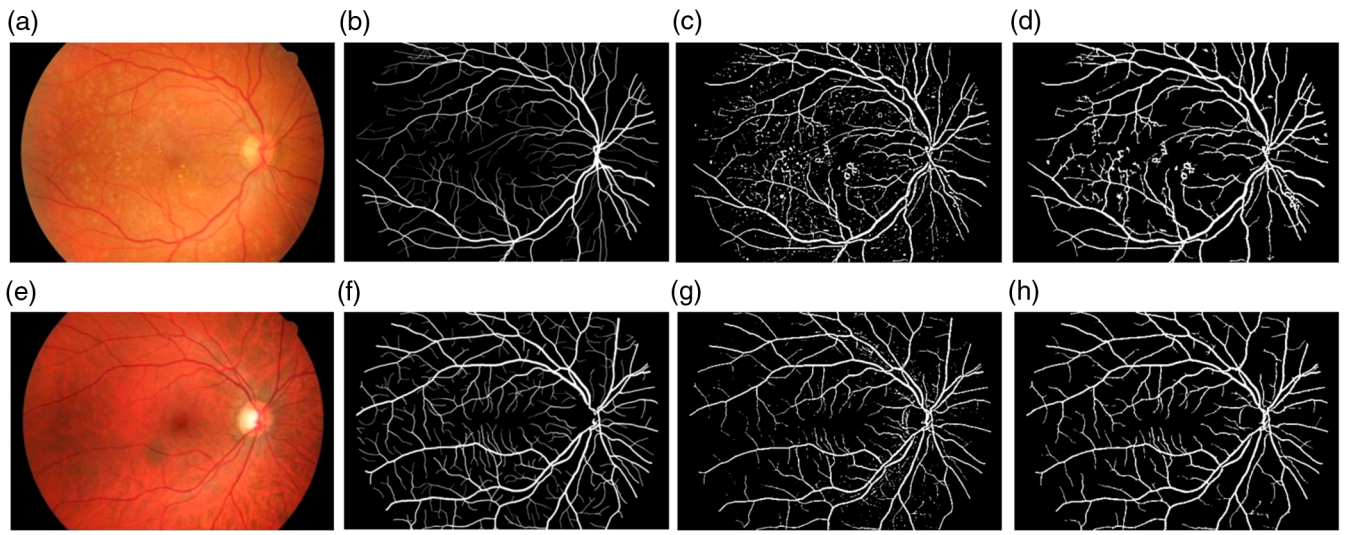

Fig. 6 Full vessel segmentation examples on a diabetic and a healthy image from HRF datasets. (a) and (e) The diabetic and healthy fundus images, respectively; (b) and (f) ground-truth segmentation images; (c) and (g) the segmentation results by the MSLD method; while (d) and (h) the segmentation results by the proposed method.

Table 2 Performance comparison of different methods on the test set in terms of sensitivity, specificity, and accuracy.

Method	Sensitivity ($\mu \pm \sigma$)	Specificity ($\mu \pm \sigma$)	Accuracy ($\mu \pm \sigma$)	Time (min)	System
Frangi et al.[45]	60.55% ± 6.52%	98.05% ± 2.25%	95.05% ± 2.05%	0.65	2.3 GHz, 4-GB RAM
Yu et al.[46]	77.89%	96.96%	95.13%	—	—
Budai et al.[28]	66.00%	98.45%	95.80%	0.44	2.3 GHz, 4-GB RAM
Odstrcilik et al.[40]	76.62%	96.84%	94.92%	18	2.3 GHz, 4-GB RAM
Nguyen et al.[26]	82.58 ± 3.65%	95.40% ± 2.14%	94.13% ± 2.14%	3.31	2.6 GHz, 4-GB RAM
Hannink et al.[47]	79.85% ± 5.02%	97.55% ± 2.01%	96.10% ± 1.7%	—	
Annunziata et al.[48]	69.08%	98.61%	95.70%	—	—
Christodoulidis et al.[36]	85.06% ± 4.03%	95.82% ± 1.15%	94.79% ± 1.06%	18.31	2.6 GHz, 4-GB RAM-
Proposed method*	87.09% ± 3.46%	95.40% ± 1.78%	94.54% ± 1.51%	3.27	2.6 GHz, 4-GB RAM

*$p < 0.05$, two sample t-test.

method detected more vessels, large and thin, with less background noise than the MSLD method.

Table 2 demonstrates the performance of the proposed method compared to other existing methods on the high-resolution database. We can observe that the sensitivity rate of the proposed vessel segmentation method is higher than most of the other methods on the test set. In comparison to a recently proposed algorithm based on the combination of the MSLD with a perceptual organization approach,[36] the specificity and accuracy rates are similar for both methods; however, the sensitivity rate is higher for the proposed method by 2.03%. Moreover, the segmentation accuracy of the proposed method is comparable to most of the other methods, achieving a rate around 95%. Hannink et al.[47] managed to obtain slightly better accuracy than our method; however, at the expense of a considerable lower sensitivity rate.

For a fair comparison, we implemented and executed the methods that are based on the MSLD approach, such as Nguyen et al.[26] and Christodoulidis et al.[36] approaches, on the same computer. We can observe from Table 2 that the computational time of the proposed method is slightly better than the MSLD method.[26] Compared to Christodoulidis method, the computational time is significantly lower for the proposed approach, segmenting the vessels approximately six times faster. The other hybrid methods rely on the use of several steps to achieve the final segmentation, which increases their overall computational time.

Small and large vessels analysis comparison. In this section, we focus further on the performance analysis of two different categories of vessels in the images: the small and the large vessels. This is necessary because there is population inhomogeneity in the different categories of vessels.[17] The standard discrepancy metrics, therefore, are not able to quantify properly the performance on the smallest category of vessel when all the vessels are considered. The different categories of vessels were considered and analyzed separately. In the context of the high-resolution data, and for the HRF database more particularly, we considered that vessel pixels belonging to vessels with diameter less than 8 pixels ($D \leq 8$ pixels) are small. We evaluated the performance of the proposed method on the healthy (H) and the diabetic (DR) data separately. The same threshold values used for the global performance analysis (Sec. 3.2.1) were used separately for the small and large vessels analysis.

Table 3 gives the performance evaluation on the small vessels in each image group. We can see that the performances on the different individual measures were higher for the proposed method compared to the MSLD method with ($p < 0.05$, two sample t-test). At a similar specificity rate, the proposed method improved the sensitivity rate by 11.02% for the healthy and by 4.42% for diabetic cases, respectively.

Figures 7 and 8 show examples from healthy and diabetic cases, where the analysis focuses on the smallest vessels. The segmented vasculature is colored according to the confusion matrix: white pixels represent the TPs, black pixels are

Table 3 Performance evaluation on the small vessels ($D \leq 8$ pixels) on the healthy and diabetic images using the standard discrepancy measures.

	Method	Sensitivity ($\mu \pm \sigma$)	Specificity ($\mu \pm \sigma$)	Accuracy ($\mu \pm \sigma$)
H	MSLD method	52.80% ± 8.64%	97.61% ± 0.51%	96.51% ± 0.63%
	Proposed method	63.82% ± 8.38%	97.38% ± 0.41%	96.52% ± 0.40%
DR	MSLD method	65.83% ± 6.64%	94.40% ± 1.36%	93.60% ± 1.21%
	Proposed method	70.25% ± 7.10%	94.1% ± 0.79%	93.49% ± 0.76%

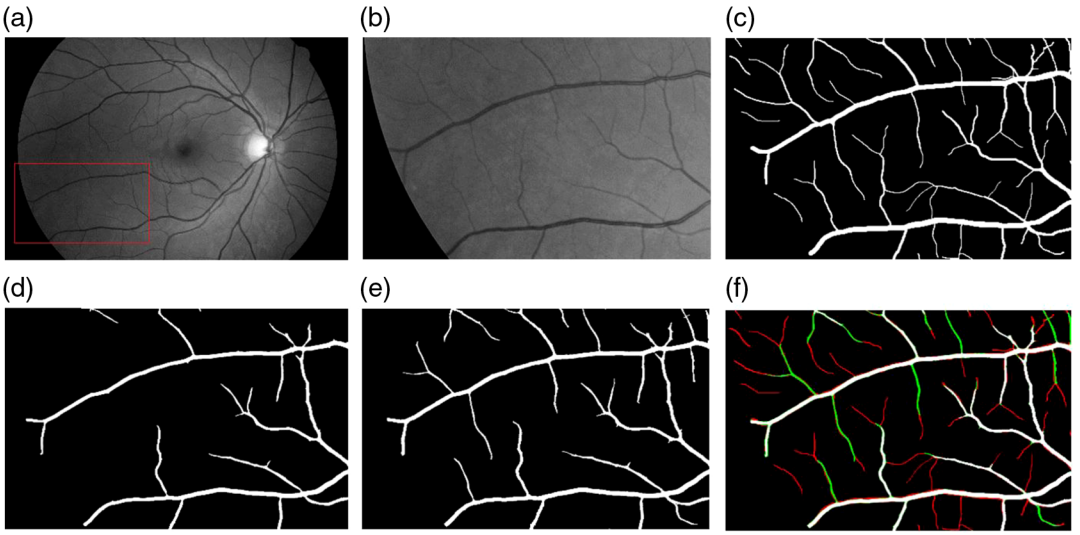

Fig. 7 Small-vessel segmentation example in healthy image from HRF datasets. (a) Grayscale input image; (b) zoomed region corresponding to inset in (a); (c) zoomed region of the manual segmentation; (d) MSLD segmentation result; (e) our segmentation result; and (f) the fusion between the manual segmentation and the proposed method segmentation result (the interpretation of each color in (f) is presented above in this section).

the TNs, blue pixels are the FPs, and red pixels are the FNs. Green pixels in Fig. 7(f) are the TPs detected by the proposed algorithm but missed by the MSLD method. Qualitatively, for the healthy case (Fig. 7), the proposed method segmented more small vessels compared to the MSLD method (sensitivity: 80.52% versus 74.98%) at a similarl background noise level (specificity: 97.78% versus 97.87%). To evaluate even further whether the proposed method segments more small vessels than the MSLD method, we include Fig. 8, which corresponds to a diabetic case. At the periphery of this image, there are many convoluted vessels that could be neovessels. From the results, we can see that the proposed method managed to include many more thin and tortuous vessels compared to the MSLD method (sensitivity: 75.85% versus 73.67%). However, in our method, small FP vessels were either reconnected to the main vasculature [see blue vessels in Fig. 8(g)] or their

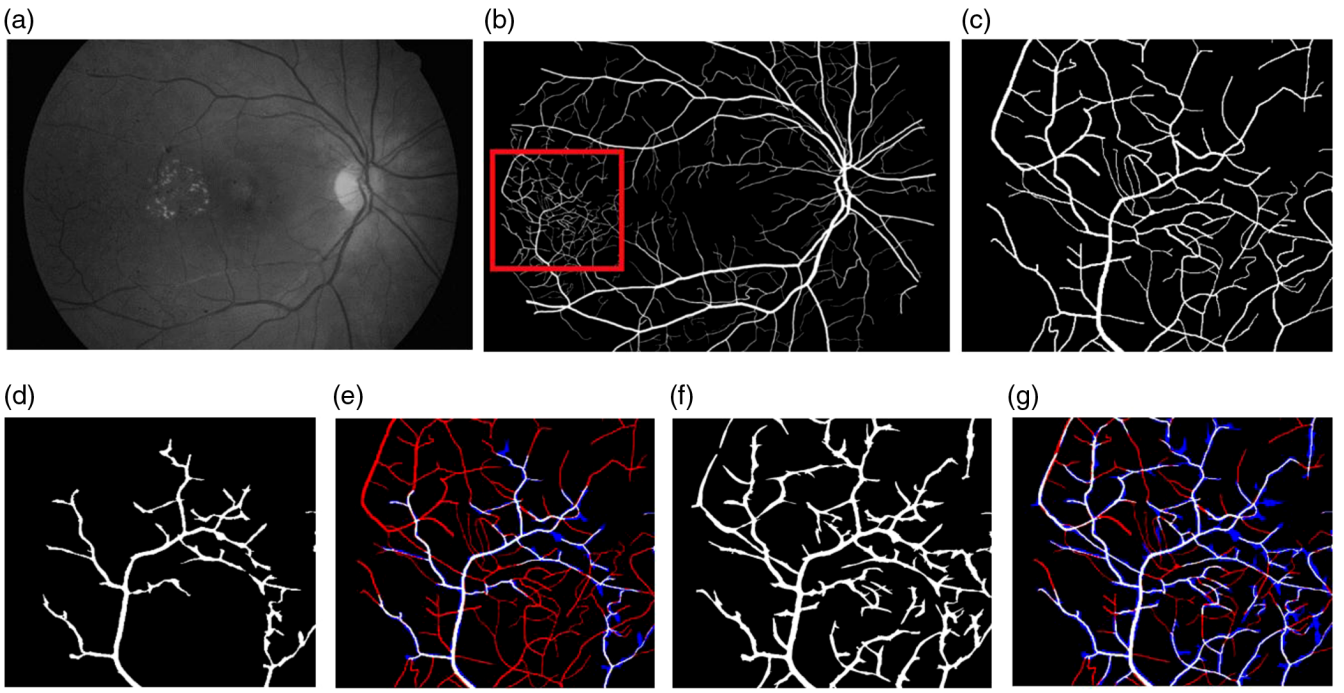

Fig. 8 Small-vessel segmentation example in a diabetic case. (a) Grayscale input image; (b) manual segmentation; (c) zoomed region of the manual segmentation; (d) and (f) the MSLD and the proposed method segmentation results; (e) and (g) the fusion between the manual segmentation and the MSLD and the proposed method segmentation results (the interpretation of each color in these figures are presented above in this section).

Table 4 Performance evaluation for the large vessels ($D > 8$ pixels) on the healthy and diabetic images using the standard discrepancy measures

Method		Sensitivity ($\mu \pm \sigma$)	Specificity ($\mu \pm \sigma$)	Accuracy ($\mu \pm \sigma$)
H	MSLD method	$0.870 \pm 3.42\%$	$0.977 \pm 0.53\%$	$0.968 \pm 0.60\%$
	Proposed method	$0.936 \pm 2.75\%$	$0.970 \pm 0.40\%$	$0.968 \pm 0.36\%$
DR	MSLD method	$0.886 \pm 2.71\%$	$0.942 \pm 1.32\%$	$0.939 \pm 1.32\%$
	Proposed method	$0.944 \pm 2.24\%$	$0.940 \pm 0.79\%$	$0.939 \pm 0.77\%$

boundaries were overestimated. The straight-line pattern of the basic line detector was not able to approximate difficult cases such as those encountered in convoluted vessels.

Table 4 gives the performance evaluation for the large vessels in each image category. In this table, we show that the specificity and the accuracy were equivalent in both methods. The sensitivity rate was significantly higher for our method compared to the MSLD method ($p < 0.05$, two sample t-test). The improvement in the sensitivity rate for the healthy and the diabetic cases were 6.6% and 6.2%, respectively. Figure 9 provides an example where the analysis focuses on the large vessels. Qualitatively, our method segmented most of the large vessels [see Fig. 9(g)] in comparison with the MSLD method [see Fig. 9(d)]. However, some FP vessels were reconnected to the main vasculature by the proposed method (blue pixels in image g).

3.2.2 *Performance evaluation on the low-resolution datasets*

For the low-resolution images, the proposed algorithm grouped the scales into two groups: $L_1 = (1, 5, 7, 9\}$ and $L_2 = \{11, 13, 15\}$. The first group threshold it by 0.70 and the second one by 0.95. The number of utilized scales was reduced by one (eight to seven scales) compared to the MSLD method. To examine which method identifies more vessel pixels, the optimized or the MSLD, we determined a threshold value ($T > 0.52$) for the MSLD with respect to the rate of identified vessels at the same background noise level (specificity), and then we compared their sensitivities.

From Tables 5 and 6, we show that the performance on the different considered measures were higher for the proposed version compared to the MSLD method ($p < 0.05$, two sample t-test). The proposed method improved the sensitivity rate against the MSLD by 4.7% for DRIVE and 1.8% for STARE datasets, respectively. The higher sensitivity rate in the two datasets indicates that the proposed method segments more retinal vessels.

Table 7 presents the performance comparison against other existing supervised and unsupervised approaches. The proposed vessel segmentation method outperformed all the existing metaheuristics vessel segmentation algorithms in the literature,[30–34] and also it obtained results comparable to the other existing methods in term of specificity and accuracy, except for the

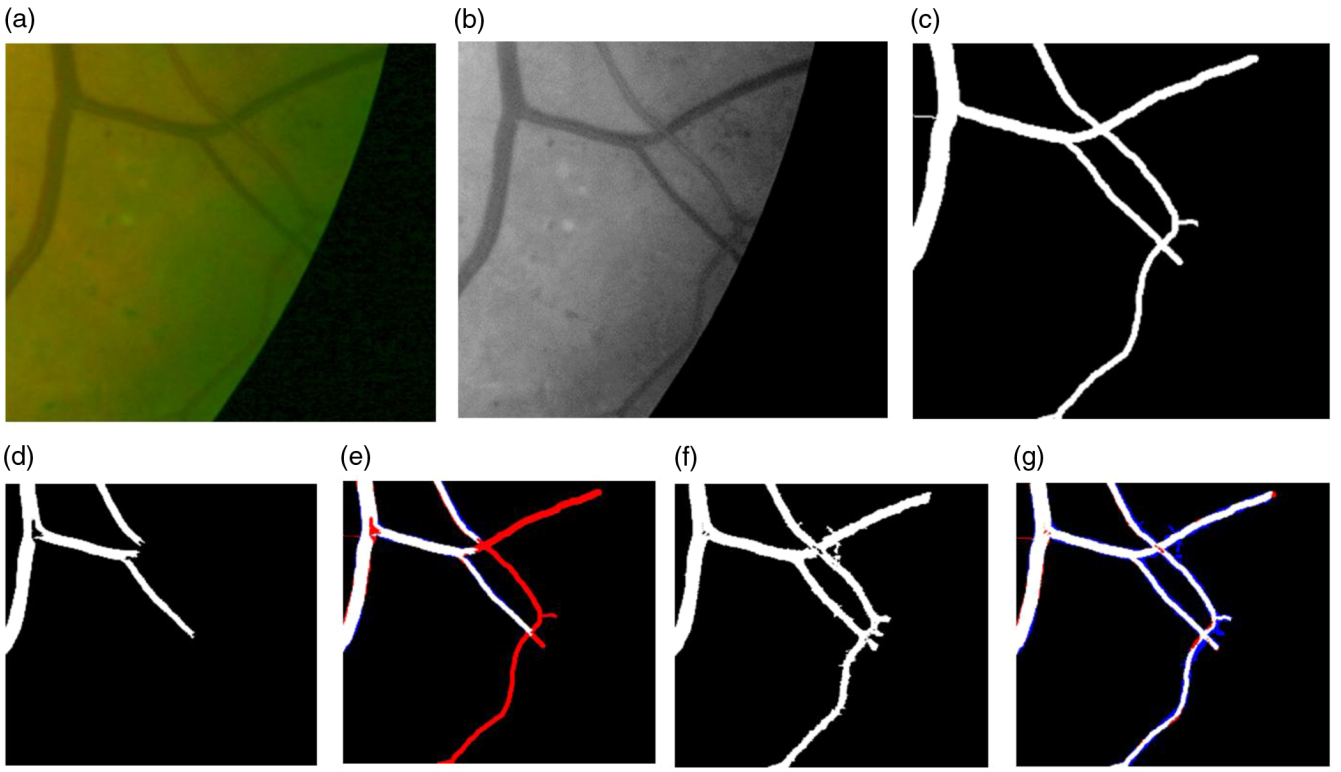

Fig. 9 Large-vessel segmentation example. (a) Zoomed region from a retinal image; (b) grayscale image of the input (a); (c) zoomed region of the manual segmentation; (d) and (f) the MSLD and the proposed method segmentation results; (e) and (g) are the fusion between the manual segmentation and the MSLD and the proposed method segmentation results.

Table 5 Performance of the proposed and the MSLD methods on the DRIVE database.

Method	Sensitivity ($\mu \pm \sigma$)	Specificity ($\mu \pm \sigma$)	Accuracy ($\mu \pm \sigma$)	Time (s)
MSLD method	0.698 ± 5.36	0.972 ± 2.02	0.941 ± 1.86	4.31
Proposed method	0.745 ± 4.26	0.971 ± 0.72	0.942 ± 0.57	4.27

Table 6 Performance of the proposed and the MSLD methods on the STARE database.

Method	Sensitivity ($\mu \pm \sigma$)	Specificity ($\mu \pm \sigma$)	Accuracy ($\mu \pm \sigma$)	Time (s)
MSLD method	0.836 ± 7.14	0.945 ± 2.58	0.932 ± 1.82	5.42
Proposed method	$0.854 \pm 6.91\%$	$0.944 \pm 1.23\%$	0.935 ± 1.53	5.35

supervised approaches[18,19] on the STARE dataset. The approach of Staal et al.[19] seems to be better than our method; however, it suffers from higher computational complexity to find the vessels. Additionally, in the proposed method we used only the DRIVE training dataset to tune the parameters, whereas most of the existing unsupervised and supervised methods used both DRIVE and STARE datasets to find the best parameters.

In addition, we can observe from Tables 5 and 6 that the execution time was reduced slightly by ~0.03 s compared to the MSLD method.[26] The reason for that is that the number of used scales in the proposed method was reduced by only one compared to the MSLD method. On the other hand, from Table 7, the computational time of the proposed vessel segmentation method was lower than most of the existing methods in the literature.

Finally, the application of the optimization metaheuristic algorithms for any problem requires the definition of the two following parameters: the objective functions and the representation of the solution. In our case, we have well defined these two parameters for the PSO algorithm, but we could easily adapt it for another optimization algorithm such as ABC. Thus, the proposed scheme could work with any heuristic optimization technique instead of PSO algorithm, but the performance of the algorithm may be affected.

4 Conclusion

In this paper, a new method for extracting blood vessels from retinal images was presented. The proposed method exploits the power of the PSO technique to find the best arrangement of scales in the MSLD method and to handle the problem of the scale response recombination. The performance of the proposed method was evaluated on two low-resolution (DRIVE and STARE) and one HRF image datasets. The data included healthy (H) and DR cases. According to the low-resolution data, the proposed method achieved significantly better

Table 7 Comparison of performance with the available segmentation methods on the STARE and DRIVE databases.

Test data	DRIVE				STARE				
Method	Sen	Spec	Acc	Time (s)	Sen	Spec	Acc	Time (s)	System
Supervised									
Marin et al.[18]	70.6%	98.0%	94.5%	90	69.4%	98.1%	95.2%	90	2.13 GHz, 2-GB RAM
Staal et al.[19]	71.9%	97.7%	94.4%	900	69.7%	98.1%	95.2%	900	1.0 GHz, 1-GB RAM
Soares et al.[21]	73.3%	97.8%	94.6%	180	72.0%	97.5%	94.8%	180	2.17 GHz, 1-GB RAM
Mendonca et al.[23]	73.4%	97.6%	94.5%	150	69.9%	97.3%	94.4%	180	3.2 GHz, 1-GB RAM
Budai et al.[28]	64.4%	98.7%	95.7%	5	58.0%	98.2%	93.8%	6	2.3 GHz, 4-GB RAM
Unsupervised									
Hoover et al.[25]	—	—	—	—	65.0%	81.0%	92.8%	300	2.6 GHz, 4-GB RAM
Miri et al.[49]	71.5%	97.6%	94.3%	50	—	—	—	—	3 GHz, 1-GB RAM
Emary et al.[32]	62.8%	98.4%	93.8%	—	58.6%	98.7%	94.4%	—	-
Asad et al.[31]	—	—	—	—	85.3%	92.1%	91.3%	42	2.53 GHz, 3-GB RAM
Cinsdikici et al.[30]	—	—	92.9%	35	—	—	—	—	—
Hassanien et al.[33]	72.1%	97.1%	93.8%	86	64.9%	98.2%	94.6%	86	—
Emary et al.[34]	—	—	93.6%	102	—	—	—	—	—
Proposed method	74.5%	97.1%	94.2%	4.27	85.4%	94.4%	93.5%	5.35	2.6 GHz, 4-GB RAM

performance compared to the MSLD method and to all existing metaheuristics vessel segmentation algorithms.

Moreover, the performance of the proposed method was evaluated qualitatively and quantitatively on the high-resolution images according to two strategies: first, when the full vasculature was considered and second, by separating the large and the small vessels. According to the results, the proposed method managed to include more thin and tortuous vessels compared to the MSLD method, by using fewer scales with different pixel resolutions, which makes the proposed method a suitable tool compared to state-of-the-art techniques. In future work, we will improve this method by including more objective functions based on perceptually important characteristics of the segmented vessels. These measures could include that recently proposed by Gegundez-Arias et al.,[50] where three measures based on connectivity, area, and length are combined. The ultimate goal is to improve further the MSLD algorithm in order to extract more tortuous structures around the optic disc or to improve the detection of pathological vessels related to sight-threatening complications, such as neovascularization.

Disclosures

The authors have no relevant financial interests in this article and no potential conflicts of interest to disclose.

References

1. J. J. Wang et al., "Retinal vessel diameter and cardiovascular mortality: pooled data analysis from two older populations," *Eur. Heart J.* **28**(16), 1984–1992 (2007).
2. T. A. Ciulla, A. G. Amador, and B. Zinman, "Diabetic retinopathy and diabetic macular edema pathophysiology, screening, and novel therapies," *Diabetes Care* **26**(9), 2653–2664 (2003).
3. A. S. Neubauer et al., "Retinal vessel analysis reproducibility in assessing cardiovascular disease," *Optom. Vision Sci.* **85**(4), E247–E254 (2008).
4. World Health Organization, "Prevention of blindness from diabetes mellitus: report of a WHO consultation in Geneva, Switzerland," (2006).
5. A. Sopharak, B. Uyyanonvara, and S. Barman, "Simple hybrid method for fine microaneurysm detection from non-dilated diabetic retinopathy retinal images," *Comput. Med. Imaging Graphics* **37**(5), 394–402 (2013).
6. C. Heneghan et al., "Characterization of changes in blood vessel width and tortuosity in retinopathy of prematurity using image analysis," *Med. Image Anal.* **6**(4), 407–429 (2002).
7. J. Lowell et al., "Measurement of retinal vessel widths from fundus images based on 2-D modeling," *IEEE Trans. Med. Imaging* **23**(10), 1196–1204 (2004).
8. A. Haddouche et al., "Detection of the foveal avascular zone on retinal angiograms using Markov randomises," *Digital Signal Process.* **20**(1), 149–154 (2010).
9. Y. Hatanaka et al., "Automated detection algorithm for arteriolar narrowing on fundus images," in *27th Annual Int. Conf. of the Engineering in Medicine and Biology Society, IEEE-EMBS 2005*, pp. 286–289, IEEE (2006).
10. E. Grisan and A. Ruggeri, "A divide et impera strategy for automatic classification of retinal vessels into arteries and veins," in *Proc. of the 25th Annual Int. Conf. of the IEEE Engineering in Medicine and Biology Society*, Vol. 1, pp. 890–893, IEEE (2003).
11. L. Seoud et al., "Red lesion detection using dynamic shape features for diabetic retinopathy screening," *IEEE Trans. Med. Imaging* **35**(4), 1116–1126 (2016).
12. S. Lahmiri and A. Shmuel, "Variational mode decomposition based approach for accurate classification of color fundus images with hemorrhages," *Opt. Laser Technol.* **96**, 243–248 (2017).
13. S. Lahmiri and M. Boukadoum, "Automated detection of circinate exudates in retina digital images using empirical mode decomposition and the entropy and uniformity of the intrinsic mode functions," *Biomed. Eng./Biomed. Tech.* **59**(4), 357–366 (2014).
14. S. Lahmiri, C. S. Gargour, and M. Gabrea, "Automated pathologies detection in retina digital images based on complex continuous wavelet transform phase angles," *Healthcare Technol. Lett.* **1**(4), 104–108 (2014).
15. M. J. Van Grinsven et al., "Fast convolutional neural network training using selective data sampling: application to hemorrhage detection in color fundus images," *IEEE Trans. Med. Imaging* **35**(5), 1273–1284 (2016).
16. M. M. Fraz et al., "Blood vessel segmentation methodologies in retinal images: a survey," *Comput. Methods Programs Biomed.* **108**(1), 407–433 (2012).
17. E. Ricci and R. Perfetti, "Retinal blood vessel segmentation using line operators and support vector classification," *IEEE Trans. Med. Imaging* **26**(10), 1357–1365 (2007).
18. D. Marin et al., "A new supervised method for blood vessel segmentation in retinal images by using gray-level and moment invariants-based features," *IEEE Trans. Med. Imaging* **30**(1), 146–158 (2011).
19. J. Staal et al., "Ridge-based vessel segmentation in color images of the retina," *IEEE Trans. Med. Imaging* **23**(4), 501–509 (2004).
20. R. Vega et al., "Retinal vessel extraction using lattice neural networks with dendritic processing," *Comput. Biol. Med.* **58**, 20–30 (2015).
21. J. V. Soares et al., "Retinal vessel segmentation using the 2-D Gabor wavelet and supervised classification," *IEEE Trans. Med. Imaging* **25**(9), 1214–1222 (2006).
22. K.-K. Maninis et al., "Deep retinal image understanding," in *Int. Conf. on Medical Image Computing and Computer-Assisted Intervention*, pp. 140–148, Springer (2016).
23. A. M. Mendonca and A. Campilho, "Segmentation of retinal blood vessels by combining the detection of centerlines and morphological reconstruction," *IEEE Trans. Med. Imaging* **25**(9), 1200–1213 (2006).
24. B. S. Lam, Y. Gao, and A. W. C. Liew, "General retinal vessel segmentation using regularization-based multiconcavity modeling," *IEEE Trans. Med. Imaging* **29**(7), 1369–1381 (2010).
25. A. Hoover, V. Kouznetsova, and M. Goldbaum, "Locating blood vessels in retinal images by piecewise threshold probing of a matched filter response," *IEEE Trans. Med. Imaging* **19**(3), 203–210 (2000).
26. U. T. Nguyen et al., "An effective retinal blood vessel segmentation method using multi-scale line detection," *Pattern Recogn.* **46**(3), 703–715 (2013).
27. O. Chutatape, L. Zheng, and S. Krishnan, "Retinal blood vessel detection and tracking by matched Gaussian and Kalman filters," in *Proc. of the 20th Annual Int. Conf. of the IEEE Engineering in Medicine and Biology Society*, Vol. 6, pp. 3144–3149, IEEE (1998).
28. A. Budai et al., "Robust vessel segmentation in fundus images," *Int. J. Biomed. Imaging* **2013**, 154860 (2013).
29. M. Al-Rawi and H. Karajeh, "Genetic algorithm matched filter optimization for automated detection of blood vessels from digital retinal images," *Comput. Methods Programs Biomed.* **87**(3), 248–253 (2007).
30. M. G. Cinsdikici and D. Aydın, "Detection of blood vessels in ophthalmoscope images using mf/ant (matched filter/ant colony) algorithm," *Comput. Methods Programs Biomed.* **96**(2), 85–95 (2009).
31. A. Asad et al., "Ant colony based feature selection heuristics for retinal vessel segmentation," arXiv:1403.1735 (2014).
32. E. Emary et al., "Retinal vessel segmentation based on possibilistic fuzzy c-means clustering optimised with cuckoo search," in *Int. Joint Conf. on Neural Networks (IJCNN)*, pp. 1792–1796, IEEE (2014).
33. A. E. Hassanien, E. Emary, and H. M. Zawbaa, "Retinal blood vessel localization approach based on bee colony swarm optimization, fuzzy c-means and pattern search," *J. Visual Commun. Image Represent.* **31**, 186–196 (2015).
34. E. Emary et al., "Multi-objective retinal vessel localization using flower pollination search algorithm with pattern search," *Adv. Data Anal. Classif.* **11**, 611–627 (2016).
35. R. Zwiggelaar et al., "Linear structures in mammographic images: detection and classification," *IEEE Trans. Med. Imaging* **23**(9), 1077–1086 (2004).
36. A. Christodoulidis et al., "A multi-scale tensor voting approach for small retinal vessel segmentation in high resolution fundus images," *Comput. Med. Imaging Graphics* **52**, 28–43 (2016).
37. G. Medioni and S. B. Kang, *"5" in Emerging Topics in Computer Vision*, Prentice Hall, Upper Saddle River, New Jersey (2004).

38. S. Lahmiri and M. Boukadoum, "An evaluation of particle swarm optimization techniques in segmentation of biomedical images," in *Proc. Companion Publication of the 2014 Annual Conf. on Genetic and Evolutionary Computation*, pp. 1313–1320, ACM (2014).
39. B. Khomri et al., "Particle swarm optimization approach for the segmentation of retinal vessels from fundus images," *Lect. Notes Comput. Sci.* **10317**, 551–558 (2017).
40. J. Odstrcilik et al., "Retinal vessel segmentation by improved matched filtering: evaluation on a new high-resolution fundus image database," *IET Image Process.* **7**(4), 373–383 (2013).
41. J. Kennedy and R. Eberhart, "A new optimizer using particle swarm theory," in *Proc. of the IEEE Sixth Int. Symp. on Micro Machine and Human Science*, pp. 39–43, IEEE (1995).
42. Y. Del Valle et al., "Particle swarm optimization: basic concepts, variants and applications in power systems," *IEEE Trans. Evol. Comput.* **12**(2), 171–195 (2008).
43. Y. Huo et al., "Elite-guided multi-objective artificial bee colony algorithm," *Appl. Soft Comput.* **32**, 199–210 (2015).
44. N. Otsu, "A threshold selection method from gray-level histograms," *Automatica* **11**(285–296), 23–27 (1975).
45. A. F. Frangi et al., "Multiscale vessel enhancement filtering," in *Medical Image Computing and Computer-Assisted Intervention-MICCAI-98*, pp. 130–137, Springer (1998).
46. H. Yu et al., "Fast vessel segmentation in retinal images using multiscale enhancement and second-order local entropy," *Proc. SPIE* **8315**, 83151B (2012).
47. J. Hannink, R. Duits, and E. Bekkers, "Crossing-preserving multi-scale vesselness," in *Medical Image Computing and Computer-Assisted Intervention–MICCAI 2014*, pp. 603–610, Springer (2014).
48. R. Annunziata et al., "Leveraging multiscale hessian-based enhancement with a novel exudate inpainting technique for retinal vessel segmentation," *IEEE J. Biomed. Health Inf.* **20**, 1129–1138 (2015).
49. M. S. Miri and A. Mahloojifar, "Retinal image analysis using curvelet transform and multistructure elements morphology by reconstruction," *IEEE Trans. Biomed. Eng.* **58**(5), 1183–1192 (2011).
50. M. E. Gegúndez-Arias et al., "A function for quality evaluation of retinal vessel segmentations," *IEEE Trans. Med. Imaging* **31**(2), 231–239 (2012).

Bilal Khomri is a PhD student at the University of Biskra, Algeria, where he is currently doing a doctoral internship to finalize his doctoral thesis at 4-D Imaging and Vision Laboratory (LIV4d), Polytechnique Montréal, Quebec, Canada. He received his master's degree in computer science from the University of Biskra, Algeria, in 2012. His area of interest is image processing and computer vision, medical image analysis (retinal image processing algorithms), metaheuristics, and nature-inspired computing.

Argyrios Christodoulidis is a research and development scientist in DIAGNOS Inc., Quebec, Canada. He received his PhD in computer science from the Polytechnique Montréal, Quebec, Canada, in 2017, and his master's degree in computer science from the University College London, England, in 2011. His area of interest is bio/medical image processing/analysis and computer vision.

Leila Djerou is a professor in the Computer Science Department, University Med Khider at Biskra, Algeria. She holds a graduate diploma, engineer in informatics, and postgraduate diploma: magister. She received her PhD from the University of Biskra, Algeria. Her domain of interest is emergent computing and complex systems, medical image analysis, image processing and computer vision, metaheuristics, and nature-inspired computing.

Mohamed Chaouki Babahenini is a professor in the Computer Science Department, University Med Khider at Biskra, Algeria. He holds a graduate diploma, engineer in informatics, and postgraduate diploma: magister. He received his PhD from the University of Biskra, Algeria. His domain of interest is emergent computing and complex systems, image processing and computer vision, computer graphics, and 3-D visualization.

Farida Cheriet is a professor in the computer and software engineering, École Polytechnique de Montréal, and a member of the research center of Sainte Justine Hospital in Montreal. She is an IEEE senior member. Her research interests include retinal image analysis, 3-D reconstruction, and visualization of vascular structures from multimodal images, and spatiotemporal registration of medical images. She is author or coauthor of more than 200 journal and refereed conference papers.